Journal of Magnetic Resonance 212 (2011) 109–115

Contents lists available at ScienceDirect

Journal of Magnetic Resonance

journal homepage: www.elsevier.com/locate/jmr

Relaxation of hyperpolarized ^{129}Xe in a deflating polymer bag

Harald E. Möller [a,b,*,1], Zackary I. Cleveland [b,1], Bastiaan Driehuys [b]

[a] Max Planck Institute for Human Cognitive and Brain Sciences, Stephanstr. 1a, 04103 Leipzig, Germany
[b] Center for In Vivo Microscopy, Department of Radiology, Duke University Medical Center, Durham, NC 27710, USA

ARTICLE INFO

Article history:
Received 20 April 2011
Revised 17 June 2011
Available online 25 June 2011

Keywords:
Gas-phase relaxation
Hyperpolarized ^{129}Xe
Longitudinal relaxation
Magnetic resonance imaging
Wall relaxation

ABSTRACT

In magnetic resonance imaging with hyperpolarized (HP) noble gases, data is often acquired during prolonged gas delivery from a storage reservoir. However, little is known about the extent to which relaxation within the reservoir will limit the useful acquisition time. For quantitative characterization, ^{129}Xe relaxation was studied in a bag made of polyvinyl fluoride (Tedlar). Particular emphasis was on wall relaxation, as this mechanism is expected to dominate. The HP ^{129}Xe magnetization dynamics in the deflating bag were accurately described by a model assuming dissolution of Xe in the polymer matrix and dipolar relaxation with neighboring nuclear spins. In particular, the wall relaxation rate changed linearly with the surface-to-volume ratio and exhibited a relaxivity of $\kappa = 0.392 \pm 0.008$ cm/h, which is in reasonable agreement with $\kappa = 0.331 \pm 0.051$ cm/h measured in a static Tedlar bag. Estimates for the bulk gas-phase ^{129}Xe relaxation yielded $T_1^{bulk} = 2.55 \pm 0.22$ h, which is dominated by intrinsic Xe–Xe relaxation, with small additional contributions from magnetic field inhomogeneities and oxygen-induced relaxation. Calculations based on these findings indicate that relaxation may limit HP ^{129}Xe experiments when slow gas delivery rates are employed as, for example, in mouse imaging or vascular infusion experiments.

1. Introduction

Magnetic resonance imaging (MRI) with hyperpolarized (HP) noble gases has become an important modality in both clinical and preclinical research [1]. In particular, for preclinical HP gas MRI, data is acquired at multiple time points during repeated or prolonged gas delivery—especially in high-resolution imaging of small animals, where the amount of HP gas consumed during each delivery (*e.g.*, one inhalation) is small (*e.g.*, between 0.2 ml in mice and 2–5 ml in rats) and does not represent a severe experimental limitation. Examples of preclinical applications using extended delivery of HP gases include the regional assessment of lung microstructure and function [2–8], detection of metastases [9], brain imaging [10], or vascular imaging [11].

In most preclinical studies, HP gases are produced in batches and are then subsequently stored in the gas phase. Provided that this storage period is relatively short (*e.g.*, a few minutes), it can be assumed that longitudinal relaxation within the reservoir will have only minor influence on the observed HP gas signal intensity. However, as studies begin to use longer imaging times (*e.g.*, up to 30 min), for instance to acquire higher resolution images, there is lack of knowledge about the extent to which HP gas relaxation will limit the useful acquisition time. Thus, to extend the acquisition times in meaningful ways, the magnetization in the storage reservoir must exhibit a sufficiently long longitudinal relaxation time, T_1^R. Previous work has demonstrated that sufficient signal continuity may not be achieved due to relaxation during HP gas storage in flexible fluoropolymer bags, which are used extensively in MRI [12]. Moreover, T_1^R in itself may not stay constant but rather may change while the bag is being deflated [13]. Therefore, it is critical to know T_1^R and its dependence on the experimental parameters, to predict how long experiments can be fruitfully conducted.

Certain intrinsic relaxation mechanisms are known to lead to very long longitudinal relaxation times, T_1^{int}, on the order of weeks for ^{3}He [14] and hours for ^{129}Xe [15–19]. In practice, however, T_1^R is usually limited by extrinsic mechanisms (see *e.g.*, [20]). These include contributions from paramagnetic impurities, such as molecular oxygen, diffusion through magnetic field gradients, and interactions with the reservoir walls. Characterizing these mechanisms by relaxation times $T_1^{O_2}$, T_1^G, and T_1^W, respectively, leads to a total relaxation rate inside the reservoir of

$$\frac{1}{T_1^R} = \frac{1}{T_1^{int}} + \frac{1}{T_1^{O_2}} + \frac{1}{T_1^G} + \frac{1}{T_1^W}. \quad (1)$$

Abbreviations: HP, hyperpolarized; MRI, magnetic resonance imaging; RF, radiofrequency; SNR, signal-to-noise ratio.

* Corresponding author at: Max Planck Institute for Human Cognitive and Brain Sciences, Stephanstr. 1a, 04103 Leipzig, Germany. Fax: +49 341 9940 2448.
E-mail addresses: moeller@cbs.mpg.de (H.E. Möller), zackary.cleveland@duke.edu (Z.I. Cleveland), bastiaan.driehuys@duke.edu (B. Driehuys).
[1] These authors contributed equally to this work.

1090-7807/$ - see front matter © 2011 Elsevier Inc. All rights reserved.
doi:10.1016/j.jmr.2011.06.017

Nomenclature

A	surface area
a, b	variables
B_0	amplitude of the static magnetic field
i	integer
k	spatial frequency
M_0^R	longitudinal ^{129}Xe magnetization in the reservoir at thermal equilibrium
M_z^R	longitudinal ^{129}Xe magnetization in the reservoir
m	number of views per HP gas breath
N	total number of ^{129}Xe atoms in the reservoir
N_W	number of ^{129}Xe atoms on the reservoir walls
n	number of HP gas breaths
$\tilde{n}$	number of HP gas breaths required to achieve the maximum SNR
n_{max}	maximum number of HP gas breaths
R^2	coefficient of variation
T_1^{bulk}	longitudinal relaxation time in the bulk gas phase of the reservoir
T_1^{int}	intrinsic longitudinal relaxation time
T_1^G	longitudinal relaxation time due to diffusion in a magnetic field gradient
$T_1^{O_2}$	longitudinal relaxation time due to paramagnetic oxygen
T_1^R	longitudinal relaxation time inside the gas reservoir
T_1^W	longitudinal relaxation time at the walls of the gas reservoir
T_R	repetition time
t	time
V	reservoir volume
$\dot{V}$	Xe gas flow
V_T	tidal volume
κ	wall relaxivity
ξ	scaling factor
τ	time between two successive noble gas inhalations
$\phi(i)$	contribution to the image SNR from the ith noble gas inhalation
$\Psi(n)$	total image SNR after the nth noble gas inhalation
$\Psi_{ideal}(n)$	ideal image SNR for infinite T_1^R
$[G]$	density of a gas, G, in amagat

Oxygen-induced relaxation depends linearly on the O_2 density. For $[O_2] = 1$ amg (1 amg = 2.687×10^{19} cm^{-3} is the density of an ideal gas at 1 atm and 0 °C) and room temperature, $T_1^{O_2} = 2.22$ s for ^{3}He [21] and 2.04 s for ^{129}Xe at low field [22]. Careful evacuation and purging of the reservoir prior to HP gas storage is thus required to reduce $1/T_1^{O_2}$ to a negligible level. This leaves gradient relaxation and wall relaxation as the most important extrinsic mechanisms that practically govern most preclinical HP gas MRI studies. These two mechanisms affect ^{3}He and ^{129}Xe differently due to substantial differences in their diffusion coefficients and residence times if adsorbed on or dissolved in the container wall. Given its high diffusion coefficient, relaxation of HP ^{3}He is highly susceptible to gradient-induced contributions [20]. Gradient-induced relaxation in the fringe field of MRI magnets (*i.e.*, a typical reservoir environment) has recently been modeled and experimentally investigated yielding $T_1^G \geqslant 4.4$ min (depending on position and magnet configuration) for HP ^{3}He [20]. However, this paper also shows that ^{129}Xe is much less affected by gradient relaxation due to its much lower diffusivity. For ^{129}Xe, however, its higher solubility in polymeric materials means wall interactions are expected to dominate the relaxation. Previous investigations have shown that at ambient temperature, noble gases dissolve into glass [23–25] or coating materials [26]. For such conditions, interactions with paramagnetic centers or neighboring nuclear spins are the dominating relaxation mechanisms. Similarly, noble gas solubility in the polymer matrix causes inter-nuclear dipole–dipole relaxation in containers made of polymer materials [27].

The aim of the current study was to investigate T_1^R for HP ^{129}Xe in a realistic setting of in vivo MRI applications, that is, in the fringe field of a horizontal-bore magnet at room temperature and near atmospheric pressure. Whereas most prior relaxation studies have employed small-sized rigid vessels, here, we use a flexible bag made of polyvinyl fluoride (Tedlar; DuPont, Buffalo, NY) and investigate the ^{129}Xe magnetization dynamics during deflation to mimic a typical scenario encountered in biomedical MRI. In an extension of recent work on gradient-induced relaxation of ^{3}He [20], particular emphasis of the current study was on investigating the wall relaxation, T_1^W, of ^{129}Xe to identify conditions where this contribution is of greatest concern. In doing so, we have developed a simple analytical model that can be used to quantitatively describe the variable reservoir relaxation experienced by HP ^{129}Xe.

2. Methods

2.1. Theory

For simplicity, Eq. (1) is rewritten as

$$\frac{1}{T_1^R} = \frac{1}{T_1^{bulk}} + \frac{1}{T_1^W}, \tag{2}$$

where all contributions from relaxation in the bulk gas (*i.e.*, T_1^{int}, $T_1^{O_2}$, and T_1^G) are combined in a single time constant T_1^{bulk}. To model $1/T_1^W$ in a deflating gas reservoir made of polymer material, we adopt a model originally proposed by Jacob et al. [24] to describe noble gas relaxation on glass surfaces where dissolution of the gas into the glass is a factor. This model is based on the solubility, diffusion, and intrinsic relaxation of ^{129}Xe in the polymer. In particular, we assume that intrinsic relaxation is mediated by dipole–dipole interactions with nuclear spins in the polymer matrix (*i.e.*, ^{1}H or ^{19}F in the particular case considered here). For conditions, in which the total number of ^{129}Xe atoms in the reservoir are much greater than the number of atoms dissolved in the polymer, $N \gg N_W$, the wall relaxation rate is predicted to depend on the surface-to-volume ratio, A/V, which leads to

$$\frac{1}{T_1^R} = \frac{1}{T_1^{bulk}} + \frac{A}{V}\kappa. \tag{3}$$

κ is the wall relaxivity, which summarizes all contributions related to the physicochemical properties of the bulk polymer.

According to the Bloch equation, the time-dependent change of the longitudinal magnetization in the reservoir is given by

$$\frac{dM_z^R}{dt} = -\frac{M_z^R - M_0^R}{T_1^R}. \tag{4}$$

The magnetization at thermal equilibrium, M_0^R, can be safely ignored because $M_z^R \gg M_0^R$ (*i.e.*, $M_z^R - M_0^R \approx M_z^R$) for HP gases. For our experimental conditions (see Section 2.2), we may assume that the reservoir volume changes linearly with time according to

$$V(t) = \max[V(0) - \dot{V}t, 0], \tag{5}$$

whereas the surface area remains constant while the bag empties. $V(0)$ is the bag volume at time $t = 0$, $\dot{V}$ is the gas flow, and $\max(a, b)$ returns the larger of its two arguments a and b. The Bloch equation obtained after combining Eqs. (3)–(5) is given by

$$\frac{dM_z^R}{dt} \approx -\frac{M_z^R}{T_1^{bulk}} - \frac{A\kappa M_z^R}{V(0) - \dot{V}t} \wedge t < \frac{V(0)}{\dot{V}}. \quad (6)$$

It is solved by separation of the variables yielding

$$\ln\frac{M_z^R(t)}{M_z^R(0)} \approx -\frac{t}{T_1^{bulk}} + \frac{A\kappa}{\dot{V}} \ln\frac{V(0) - \dot{V}t}{V(0)} \wedge t < \frac{V(0)}{\dot{V}}. \quad (7)$$

Considering that the exponential of a product is the power function of the exponential, Eq. (7) can be conveniently rewritten as

$$M_z^R(t) = M_z^R(0) \exp\left(-\frac{t}{T_1^{bulk}}\right) \times \left[\frac{V(t)}{V(0)}\right]^{A\kappa/\dot{V}}. \quad (8)$$

2.2. Experimental methods

Xenon of natural abundance (26% ^{129}Xe, Airgas National Welders Inc., Durham, NC) was hyperpolarized by spin-exchange optical pumping [28] in batches between 100 and 300 ml using a prototype commercial polarizer (model 9800, MITI, Durham, NC). Briefly, a continuous flow of dilute Xe (1% Xe, 89% He, 10% N_2) was passed through an optical cell containing rubidium vapor at 433 K and a pressure of 500 kPa [29]. Following cryogenic accumulation, Xe ice was thawed into a 350-ml Tedlar bag (Jensen Inert Products, Coral Springs, FL) with final polarizations after thawing of approximately 5–10%. The bag, serving as a flexible HP gas reservoir, was made from two rectangular sheets (18.0 cm × 9.1 cm) of Tedlar film, which were sealed at the edges and had an inner surface area of approximately 328 cm^2. It was located within a Plexiglas cylinder, which was immediately placed within the fringe field ($B_0 \approx 0.1$ T) of a 2-T horizontal-bore MRI magnet and aligned with its bore.

The Tedlar bag was pressurized to approximately 1.2 kPa above ambient pressure by flowing nitrogen gas from a supply tank into the cylinder. Via polyethylene tubing (1.6-mm inner diameter), HP ^{129}Xe was passed through the radiofrequency (RF) coil, which was located approximately 1.2 m downstream of the gas reservoir. The flow of Xe out of the bag was initiated by opening a plastic stopcock and was controlled by a direct-reading gas flow meter (Cole-Parmer, Vernon Hills, IL). This flow meter was located inline between the Plexiglas cylinder and the N_2 supply tank. As only low N_2 pressure was applied, we may assume that the N_2 gas volume that entered the Plexiglas cylinder compressed the collapsing Tedlar bag such that an identical Xe volume flowed from the bag toward the RF coil. This setup achieved a sufficiently constant Xe flow without requiring additional flow restrictors [12].

^{129}Xe spectra were acquired using a 2-T horizontal, 30-cm bore magnet (Oxford Instruments, Oxford, UK) controlled by a GE EXCITE 12.0 console (GE Healthcare, Milwaukee, WI). Instead of its intrinsic 63.86-MHz frequency, the scanner was operated at 23.66 MHz using an up-down converter (Cummings Electronics Labs, North Andover, MA). An integrated transmit-receive switch with a 31-dB gain preamplifier (Nova Medical, Wilmington, MA) was used to interface the scanner to the custom-made linear birdcage RF coil (8-cm long, 7-cm diameter). Relaxation measurements were performed employing a simple repetitive pulse-and-acquire technique with long series of evenly spaced 1° RF pulses. A total of seven experiments were performed with a single bag in the order as listed in Table 1 with different settings for the initial bag inflation volume (≈100–300 ml), Xe gas flow (2–15 ml/min), repetition time, T_R (2–10 s), and number of repetitions (400–720).

Spectra were processed using HiRes Ver. 1.6 (Hatch Center for MR Research, Columbia University, New York, NY). Further data analysis was performed with PASW Statistics 18 (SPSS Inc., Chicago, IL) and routines written in MATLAB (The MathWorks Inc., Natick, MA). The signal decay curves obtained from the integrated spectra were fitted to Eq. (8) using a Levenberg–Marquardt algorithm with $M_z^R(0)$, $V(0)$, T_1^{bulk}, and κ as free parameters.

In a separate set of experiments, 'static' ^{129}Xe relaxation measurements at 2 T (*i.e.*, in the absence of gas flow) were made after dispensing a known volume of HP ^{129}Xe (between 47 cm^3 and 226 cm^3 as estimated from the gas flow through the optical cell and the measured dead volume of the polarizer) into a second Tedlar bag with an inner surface area of 161 cm^2. Polarization decay in the sealed bag at ambient pressure was monitored by applying a series of 1° RF pulses. Relaxation rates were then calculated by non-linear least-squares fitting of the HP ^{129}Xe signal as a function of time and number of applied RF pulses.

3. Results and discussion

3.1. Quantitative characterization of relaxation

Overall, the signal decay curves measured in the first bag under conditions of flow were well described by Eq. (8). Examples of fits from individual experiments are shown in Fig. 1. Consistent results were also obtained if the combined data from all measurements were concatenated and fitted to a single set of relaxation parameters (*i.e.*, under the constrained assumption of identical T_1^{bulk} and κ for all curves). Table 1 gives a summary of all quantitative results, which in aggregate are well described by the Tedlar polymer exhibiting a wall relaxivity on the order of 0.4 cm/h. This would imply an initial wall relaxation time of approximately 2.7 h, which is of roughly the same order as the relaxation time in the bulk gas. However, T_1^W would decrease to less than 5 min when the bag has deflated to a volume of 10 ml. To illustrate, Fig. 2 shows an estimate of T_1^R, including the fixed contribution from relaxation in

Table 1
Fitting results (R^2 is the coefficient of determination).

Exp.	$\dot{V}$(ml/min)	T_R (s)	$M_z^R(0)$(a.u.)	$V(0)$ (ml)	T_1^{bulk}(h)	κ (cm/h)	R^2
1	2	10	607.0 ± 1.7	141.9 ± 2.9	–[a]	1.14 ± 0.043	0.997
2	5	5	1976.8 ± 5.7	118.1 ± 0.1	–[a]	0.411 ± 0.009	0.998
3	10	2.5	1730.0 ± 10.4	137.6 ± 0.2	–[a]	0.175 ± 0.016	0.987
4	7.5	3	1902.4 ± 9.3	122.4 ± 0.1	–[a]	0.361 ± 0.014	0.989
5	15	2	2455.2 ± 9.0	138.0 ± 0.0	–[a]	0.468 ± 0.011	0.993
6	5	5	1959.5 ± 9.1	249.9 ± 2.2	–[a]	1.054 ± 0.026	0.984
7	10	5	1793.1 ± 4.0	251.2 ± 0.2	–[a]	0.758 ± 0.013	0.999
Combined analysis[b]:					**2.55 ± 0.22**	**0.392 ± 0.008**	0.987

[a] No reliable result obtained from fit (error estimate exceeded fitted value).
[b] Simultaneous fit to the combined data from all experiments.

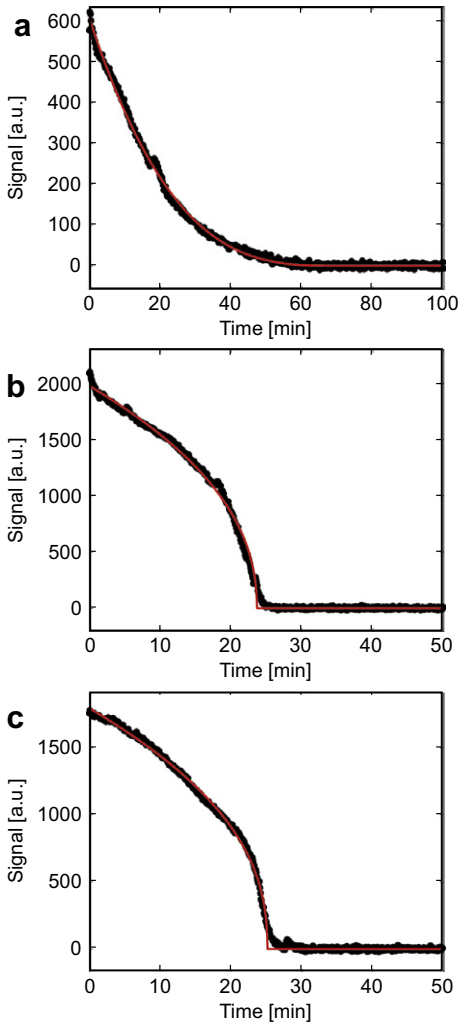

Fig. 1. Examples of fitting results obtained in experiments with different flow rates and repetition times (black circles: experimental data; red solid lines: fitted decays). Depolarization occurring within the bag is measured by observing the intensity of HP ^{129}Xe signal as it flows through the RF coil. (a) Experiment 1 with $\dot{V} = 2$ ml/s, $T_R = 10$ s; (b) Exp. 2 with $\dot{V} = 5$ ml/s, $T_R = 5$ s; (c) Exp. 7 with $\dot{V} = 10$ ml/s, $T_R = 5$ s.

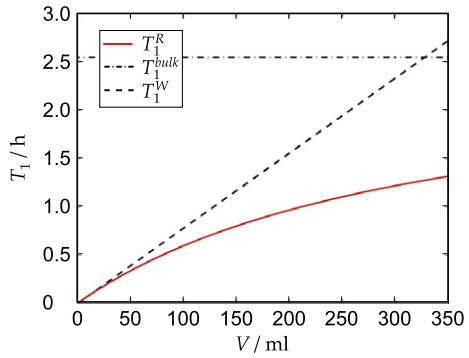

Fig. 2. Variation of the relaxation times, T_1^R (red solid line), T_1^{bulk} (black dash-dotted line), and T_1^W (black dashed line) as a function of the reservoir volume computed with Eq. (3) in conjunction with the result from the constrained fit of the combined data, $T_1^{bulk} = 2.55 \pm 0.22$ h; $\kappa = 0.392 \pm 0.008$ cm/h. (For interpretation of the references to colour in this figure legend, the reader is referred to the web version of this article.)

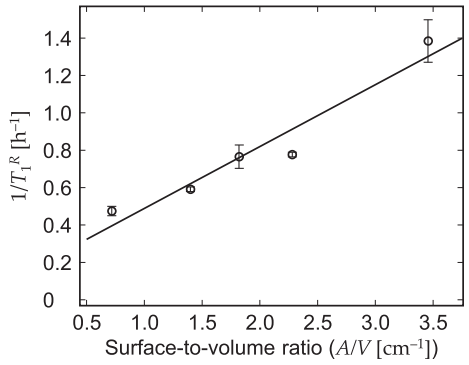

Fig. 3. Relaxation rates, $1/T_1^R$, recorded at 2 T as a function of the surface-to-volume ratio in a single sealed Tedlar bag that had been filled with different volumes of HP ^{129}Xe (static conditions). The solid line is a linear fit ($R^2 = 0.993$) to Eq. (3) yielding $1/T_1^{bulk} = 0.16 \pm 0.11$ h^{-1} and $\kappa = 0.331 \pm 0.051$ cm/h.

the bulk gas, T_1^{bulk}, and the variable wall-relaxation contribution, T_1^W, as a function of the reservoir volume.

The results also enable estimates of ^{129}Xe relaxation by mechanisms other than wall relaxation. As expected, these mechanisms only modestly contributed to the overall decay. We were able to extract estimates for the gas-phase ^{129}Xe relaxation, T_1^{bulk}, from the constrained fit of the combined data yielding $T_1^{bulk} = 2.55 \pm 0.22$ h. It is instructive to compare this result to the estimated wall relaxivity: pure gas-phase relaxation gives rise to a 10% decay of the initial signal after approximately 16 min. However, wall mechanisms lead to relaxation rates exceeding $1/T_1^{bulk}$ by a factors of 3 or 11 after 16 min in experiments performed with flow rates of 2 ml/min or 10 ml/min, respectively. As wall relaxation already dominates during the early phase of the experiments and progressively gains importance, it is intrinsically difficult to separate T_1^{bulk} with sufficient precision in a single experiment. The obtained value of T_1^{bulk} is somewhat less than the expected intrinsic relaxation time of $T_1^{int} = 4.1$ h [19], and the remaining difference may be due to contributions from paramagnetic oxygen, $T_1^{O_2}$, and gradient effects, T_1^G. We can estimate T_1^G from the work of Zheng et al. [20]. They found a ^{3}He relaxation time of $T_1^G \approx 22.6$ min at 1.2 m from the magnet isocenter, which was the position of the Xe reservoir used in our current study. With the known ratio of the diffusion coefficients for ^{3}He and ^{129}Xe (2.0/0.0571 ≈ 35 [20]), this yields $T_1^G \approx 13.2$ h for ^{129}Xe. Combining the above data with Eqs. (1) and (2) leads to an estimate of the remaining relaxation due to oxygen of $T_1^{O_2} \approx 13.3$ h. With the assumption of a relaxivity of 0.491 s^{-1} amg^{-1} [22], this suggests $[O_2] \approx 4.2 \times 10^{-5}$ amg as a typical degree of contamination by O_2 in our experiments, which is equivalent to a partial pressure of 0.046 mbar at 293 K.

According to Eq. (3), the relaxivity κ (expressed in cm/h) is equivalent to the wall relaxation rate (in h^{-1}) for a hypothetical surface-to-volume ratio of $A/V = 1$ cm^{-1}. The value of $\kappa = 0.392 \pm 0.008$ cm/h obtained from the constrained fit of all data recorded in the first bag during deflating in the fringe field (≈0.1 T) is corroborated by the 'static' experiments performed with the second bag in a homogeneous field of 2 T. Fig. 3 shows the measured relaxation rate as a function of the surface-to-volume ratio and a linear fit to Eq. (3) yielding $\kappa = 0.331 \pm 0.051$ cm/h. The good agreement between both types of experiments suggests that κ only weakly depends on the magnetic field strength or magnetic field gradients and is relatively consistent between bags. Note that T_1^{bulk} obtained by extrapolation to $A/V = 0$ is prone to errors in the volume adjustment, which might result from a slight miscalibration of the gas flow through the polarizer, whereas the determination of κ from the slope of the linear fit is relatively robust. The estimation of $T_1^{bulk} \approx 6.3 \pm 4.3$ h from the static experiment was thus associated with a large error.

Table 1 indicates that the variations in κ between individual flow experiments substantially exceeded the statistical errors of the fits. Correlations of κ with the gas flow rate and the order of the experiments were weak and insignificant ($R^2 = 0.32$; $P = 0.19$ and $R^2 = 0.0083$; $P = 0.85$, respectively). Hence, within the experimental accuracy, there were no indications of a systematic change in relaxivity related to repeated use of a bag. Variation in κ might result from varying degrees of impurities (*e.g.*, paramagnetic O_2 dissolving in the polymer when exposed to ambient air between experiments or during evacuation of the bag prior to filling). More likely, the relatively large range of variation results from random folding and collapsing of the bag during deflation. As a consequence, Xe will be exposed to an 'effective surface area', which is smaller than the geometric surface area. This leads to an underestimation of κ, which might vary between experiments. Folding of the bag might further produce a deviation from the constant-flow conditions assumed in Eq. (5). Both effects should be relevant only at small volumes. Consistently, a systematic deviation in the fitted signal curve from the experimental data is evident in Fig. 1 in the region where the bag is almost emptied (*i.e.*, for $t \to V(0)/\dot{V}$).

Another discrepancy occurs in the region of large reservoir volumes, which is readily explained by a deviation from a steady gas flow when the reservoir is first opened. Hence, the bag was at a slightly higher pressure than the ambient air at the onset of the measurements leading to a short period of relatively rapid gas flow until a steady-state pressure difference was established. This initial burst of HP ^{129}Xe had a shorter transit time and, therefore, experienced less gas-phase relaxation during the transit to the RF coil than gas arriving at later periods.

The relaxivity we report here for the Tedlar material is roughly one fourth of the $\kappa = 1.494$ cm/h reported for polytetrafluoroethylene (Teflon) [27]. According to Jacob et al. [24], the relaxivity is expected to depend on the solubility and diffusivity of ^{129}Xe in the polymer as well as on the strength of dipolar interactions with ^{1}H or ^{19}F nuclei in the polymer matrix. Compared to Teflon, which consists of $(CF_2CF_2)_n$ chains, the dipolar interaction is expected to be slightly stronger in Tedlar, which consists of $(CH_2CHF)_n$ chains, as the magnetic moment of the proton is slightly larger than that of ^{19}F. This should lead to an increased relaxivity in Tedlar. However, Tedlar has a very low permeability coefficient (*i.e.*, the product of the solubility coefficient and the diffusion coefficient) for most gases, with this being generally one to two orders of magnitude lower in Tedlar than in Teflon [30]. Hence, the favorable (*i.e.*, small) wall relaxivity in Tedlar is most likely due to a low solubility for Xe.

3.2. Implications for HP ^{129}Xe imaging

By quantifying relaxation, it is possible to predict the influence of polarization decay in the reservoir on MRI experiments. In particular, it is useful to consider a ventilation experiment with $n \geqslant 1$ HP gas breaths, a tidal volume V_T, and a breath-to-breath interval τ. If $m \geqslant 1$ views are acquired for each HP ^{129}Xe inhalation, the total number of k-space lines (or 'views') is $n \times m$. With each HP gas breath, a magnetization according to Eq. (8) is delivered to the lungs, and the contribution to the signal-to-noise ratio (SNR) from the ith breath may be written as

$$\phi(i) = \xi\sqrt{m}\exp\left[-\frac{(i-1)\tau}{T_1^{bulk}}\right] \times \left[\frac{V((i-1)\tau)}{V(0)}\right]^{A\kappa/\dot{V}}, \tag{9}$$

where ξ is a scaling factor depending on parameters such as the initial polarization, flip angle, relaxation in the lung, RF coil tuning and matching, receiver gain and bandwidth, noise power, etc. An exhaustive analysis of these factors on the SNR in HP noble gas lung MRI has been published elsewhere [31]. Assuming that the noise is random, the total image SNR after n breaths is given by

$$\Psi(n) = \frac{1}{\sqrt{n}}\sum_{i=1}^{n}\phi(i). \tag{10}$$

Note that $\Psi_{ideal}(n) = \sqrt{n}$ is obtained for the ideal case of constant ϕ (i) (*i.e.*, infinite T_1^R). In a real system, relaxation in the reservoir leads to a continuously decreasing $\phi(i)$. With increasing n, $\Psi(n)$ thus passes through a maximum and subsequently declines. Hence, the maximum at $n = \tilde{n}$ with $(\partial\Psi/\partial n)_{n=\tilde{n}} = 0$ identifies an upper limit of HP gas breaths, beyond which the added noise exceeds further signal contributions, and the sensitivity starts to decline. Considering that

$$\Psi(n+1) = \frac{\phi(n+1)}{\sqrt{n+1}} + \frac{\sqrt{n}}{\sqrt{n+1}}\Psi(n), \tag{11}$$

an alternative condition for the maximum is given by

$$\Psi(n+1) \leqslant \Psi(n) \Rightarrow \phi(n+1) \leqslant (\sqrt{n+1} - \sqrt{n})\Psi(n) \quad \text{if} \quad n = \tilde{n}. \tag{12}$$

Eq. (12) may be used for a simple graphical procedure to obtain an estimate of $\tilde{n}$ from the intersection of $\phi(n+1)$ and $(\sqrt{n+1} - \sqrt{n})\Psi(n)$ plotted versus n.

As instructive examples, we consider two ventilation imaging experiments, in which $V(0) = 900$ ml of Xe is stored in a 1000-ml Tedlar bag with a surface area of 632 cm^2 in: (i) a rat with $\tau = 1$ s (*i.e.*, 60 breaths per min) and $V_T = 2$ ml and (ii) a mouse with $\tau = 0.6$ s (*i.e.*, 100 breaths per min) and $V_T = 0.2$ ml. Assuming that the breathing gas is a mixture of 75% Xe and 25% O_2 [7], the flow rates are $\dot{V} = 1.5$ ml/s and 0.25 ml/s, which limits the maximum number of breaths to $n_{max} = 600$ and 6000, respectively. We further assume that Xe is mixed with O_2 outside of the storage bag on the route to the coil in these experiments; hence, relaxation in the reservoir is not affected by the mixing. Figs. 4 and 5b demonstrate the progress in image SNR computed with Eq. (10) in comparison to the ideal case of infinite T_1^R. During the rat experiment lasting only 10 min, $\tilde{n}$ is not reached (*i.e.*, $n_{max} < \tilde{n}$), and $\Psi(n)$ stays close to the ideal limit with an SNR of $0.93\,\Psi_{ideal}$ after 600 breaths. This indicates that relaxation is not a limiting factor under these experimental conditions. However, in the mouse experiment lasting 1 h, the final SNR after 6000 breaths is only $0.66\,\Psi_{ideal}$ due to significant polarization loss from relaxation in the reservoir. Inspection of Fig. 5b yields $\tilde{n} = 5513$. Hence, in order to maximize the SNR, signal acquisition should not be continued after this point, which corresponds to consumption of 92% of the initial volume of Xe. Note that even slower flow rates ($\dot{V} = 0.12$ ml/s) have been em-

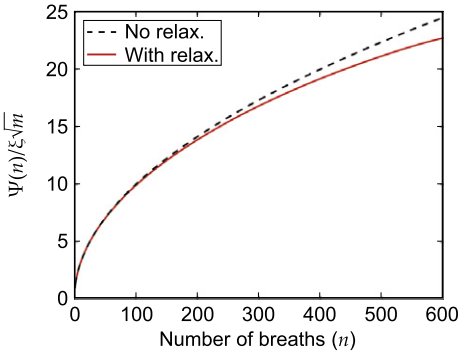

Fig. 4. Variation of the relative SNR [$\Psi(n)$ in units of $\xi\sqrt{m}$] computed with Eqs. (9) and (10) as a function of the number of Xe breaths (red solid line) in a rat ventilation study [60 breaths per min; $V(0) = 900$ ml; $\dot{V} = 1.5$ ml/s; $n_{max} = 600$; Tedlar bag with $A = 632$ cm^2] and comparison with the ideal case, $\Psi_{ideal}(n)$, without relaxation-related polarization loss in the reservoir (black dashed line). (For interpretation of the references to colour in this figure legend, the reader is referred to the web version of this article.)

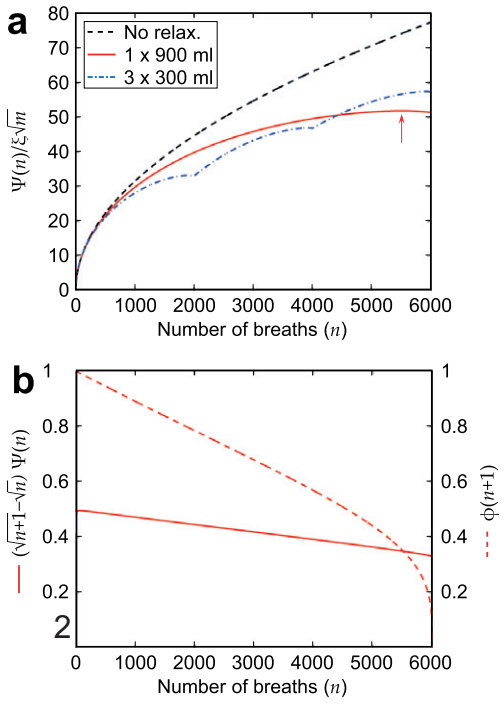

Fig. 5. (a) Variation of the relative SNR [$\Psi(n)$ in units of $\xi\sqrt{m}$] computed with Eqs. (9) and (10) as a function of the number of Xe breaths (red solid line) in a mouse ventilation study [100 breaths per min; $V(0) = 900$ ml; $\dot{V} = 0.25$ ml/s; $n_{max} = 6000$; Tedlar bag with $A = 632$ cm^2] and comparison with the ideal case, $\Psi_{ideal}(n)$, without relaxation-related polarization loss in the reservoir (black dashed line). The red arrow indicates the position of the maximum of $\Psi(n)$. The blue dash-dotted line shows $\Psi(n)$ for an alternative experiment employing three batches, each with $V(0) = 300$ ml in a Tedlar bag with $A = 328$ cm^2 and otherwise identical parameters. (b) Plots of $\phi(n+1)$ (red dotted line) and $(\sqrt{n+1} - \sqrt{n})\Psi(n)$ (red solid line) versus n for the estimation of $\bar{n}$ from the intersection of both curves. (For interpretation of the references to colour in this figure legend, the reader is referred to the web version of this article.)

ployed in recent experiments to image pulmonary perfusion by means of continuously infusing HP ^{129}Xe to the blood using a gas-exchange module and an extracorporeal circuit [32,33]. Assuming otherwise identical conditions [*i.e.*, $V(0) = 900$ ml], the SNR would already decrease after consumption of 65% of the initial volume of Xe (final SNR of $0.41\,\Psi_{ideal}$) in this case.

It is also noteworthy that a slight modification of the experimental design discussed above will result in a substantially improved SNR. That is, instead of producing and delivering a single, 900-ml batch of HP ^{129}Xe, the mouse ventilation experiment can be divided—for instance into three periods of 20 min, during which separately polarized 300-ml batches are delivered (note that 20 min allows sufficient time to polarize new 300-ml batches of HP ^{129}Xe in parallel to ongoing image acquisition). The result of such a multiple-batch approach is additionally shown in Fig. 5a, which indicates that the final SNR after 6000 breaths would be improved to $0.74\,\Psi_{ideal}$.

4. Conclusion

Longitudinal relaxation of HP ^{129}Xe in a deflating Tedlar bag is dominated by a wall relaxation rate that depends linearly on the surface-to-volume ratio, with an additional constant contribution from bulk gas-phase relaxation. This observation is consistent with a model assuming dissolution of xenon in the polymer matrix and a dipolar wall relaxation mechanism. A change of T_1^R will non-uniformly reduce the input signal over the course of raw data sampling, which may result in sub-optimal signal utilization, degrade the point-spread function, or lead to errors in quantitative MRI. Effects from relaxation in the reservoir will be more severe in studies employing small gas flow rates as, for example, in mouse imaging or HP ^{129}Xe infusion studies. However, such effects might be mitigated if the change of T_1^R is explicitly considered in the experimental design or analysis.

Acknowledgments

The authors thank Drs. G. Allan Johnson and Laurence W. Hedlund for supporting the experiments and Rosie Wallis for carefully proofreading the manuscript. This work was conducted at the Duke Center for In Vivo Microscopy, an NIH/NCRR National Biomedical Technology Research Center (P41 RR005959) with further support from NCI (R01 CA-142842).

References

[1] H.E. Möller, X.J. Chen, B. Saam, K.D. Hagspiel, G.A. Johnson, T.A. Altes, E.E. de Lange, H.U. Kauczor, MRI of the lungs using hyperpolarized noble gases, Magn. Reson. Med. 47 (2002) 1029–1051.
[2] X.J. Chen, L.W. Hedlund, H.E. Möller, M.S. Chawla, R.R. Maronpot, G.A. Johnson, Detection of emphysema in rat lungs using magnetic resonance measurements of ^{3}He diffusion, Proc. Natl. Acad. Sci. USA 97 (2000) 11478–11481.
[3] J. Mata, T.A. Altes, J. Cai, K. Ruppert, W. Mitzner, K.D. Hagspiel, B. Patel, M. Salerno, J.R. Brookeman, E.E. de Lange, W.A. Tobias, H.T.J. Wang, G.D. Cates, J.P. Mugler, Evaluation of emphysema severity and progression in a rabit model: comparison of hyperpolarized ^{3}He and ^{129}Xe diffusion MRI with lung morphometry, J. Appl. Physiol. 102 (2007) 1273–1280.
[4] K. Emami, R.V. Cadman, J.M. Woodburn, M.C. Fischer, S.J. Kadlecek, J. Zhu, S. Pickup, R.A. Guyer, M. Law, V. Vahdat, M.E. Friscia, M. Ishii, J. Yu, W.B. Gefter, J.B. Shrager, R.R. Rizi, Early changes of lung function and structure in an elastase model of emphysema—a hyperpolarized ^{3}He MRI study, J. Appl. Physiol. 104 (2008) 773–786.
[5] D.A. Yablonskiy, A.L. Sukstanskii, J.C. Woods, D.S. Gierada, J.D. Quirk, J.C. Hogg, J.D. Cooper, M.S. Conradi, Quantification of lung microstructure with hyperpolarized ^{3}He diffusion MRI, J. Appl. Physiol. 107 (2009) 1258–1265.
[6] H. Imai, A. Kimura, S. Iguchi, Y. Hori, S. Masuda, H. Fujiwara, Noninvasive detection of pulmonary tissue destruction in a mouse model of emphysema using hyperpolarized ^{129}Xe MRS under spontaneous respiration, Magn. Reson. Med. 64 (2010) 929–938.
[7] B. Driehuys, G.P. Cofer, J. Pollaro, J. Boslego Mackel, L.W. Hedlund, G.A. Johnson, Imaging alveolar–capillary gas transfer using hyperpolarized ^{129}Xe MRI, Proc. Natl. Acad. Sci. USA 103 (2006) 18278–18283.
[8] B. Driehuys, H.E. Möller, Z.I. Cleveland, J. Pollaro, L.W. Hedlund, Pulmonary perfusion and xenon gas exchange in rats: MR imaging with intravenous injection of hyperpolarized ^{129}Xe, Radiology 252 (2009) 386–393.
[9] R.T. Branca, Z.I. Cleveland, B. Fubara, C.S.S.R. Kumar, R.R. Maronpot, C. Leuschner, W.S. Warren, B. Driehuys, Molecular MRI for sensitive and specific detection of lung metastases, Proc. Natl. Acad. Sci. USA 107 (2010) 3693–3697.
[10] S.D. Swanson, M.S. Rosen, K.P. Coulter, R.C. Welsh, T.E. Chupp, Distribution and dynamics of laser-polarized ^{129}Xe magnetization in vivo, Magn. Reson. Med. 42 (1999) 1137–1145.
[11] H.E. Möller, M.S. Chawla, X.J. Chen, B. Driehuys, L.W. Hedlund, C.T. Wheeler, G.A. Johnson, Magnetic resonance angiography with hyperpolarized ^{129}Xe dissolved in a lipid emulsion, Magn. Reson. Med. 41 (1999) 1058–1064.
[12] Z.I. Cleveland, H.E. Möller, L.W. Hedlund, B. Driehuys, Continuously infusing hyperpolarized ^{129}Xe into flowing aqueous solutions using hydrophobic gas exchange membranes, J. Phys. Chem. B 113 (2009) 12489–12499.
[13] H.E. Möller, X.J. Chen, M.S. Chawla, B. Driehuys, L.W. Hedlund, G.A. Johnson, Signal dynamics in magnetic resonance imaging of the lung with hyperpolarized noble gases, J. Magn. Reson. 135 (1998) 133–143.
[14] N.R. Newbury, A.S. Barton, G.D. Cates, W. Happer, H. Middleton, Gaseous ^{3}He–^{3}He magnetic dipolar spin relaxation, Phys. Rev. A 48 (1993) 4411–4420.
[15] R.L. Streever, H.Y. Carr, Nuclear magnetic resonance of Xe ^{129}in natural xenon, Phys. Rev. 121 (1961) 20–25.
[16] H.C. Torrey, Chemical shift and relaxation of Xe ^{129}in xenon gas, Phys. Rev. 130 (1963) 2306–2312.
[17] B. Shizgal, Calculation of the NMR relaxation time of dilute ^{129}Xe gas, Chem. Phys. 5 (1974) 464–470.
[18] I.L. Moudrakovski, S.R. Breeze, B. Simard, C.I. Ratcliffe, J.A. Ripmeester, T. Seideman, J.S. Tse, G. Santyr, Gas-phase nuclear magnetic relaxation in ^{129}Xe revisited, J. Chem. Phys. 114 (2001) 2173–2181.
[19] B. Chann, I.A. Nelson, L.W. Anderson, B. Driehuys, T.G. Walker, ^{129}Xe–Xe molecular spin relaxation, Phys. Rev. Lett. 88 (2002) 113201.
[20] W. Zheng, Z.I. Cleveland, H.E. Möller, B. Driehuys, Gradient-induced longitudinal relaxation of hyperpolarized noble gases in the fringe field of superconducting magnets used for magnetic resonance, J. Magn. Reson. 208 (2011) 284–290.

[21] B. Saam, W. Happer, H. Middleton, Nuclear relaxation of ^{3}He in the presence of O_2, Phys. Rev. A 52 (1995) 862–865.
[22] C.J. Jameson, A.K. Jameson, J.K. Hwang, Nuclear spin relaxation by intermolecular magnetic dipole coupling in the gas phase. ^{129}Xe in oxygen, J. Chem. Phys. 89 (1988) 4074–4081.
[23] W.A. Fitzsimmons, L.L. Tankersley, G.K. Walters, Nature of surface-induced nuclear-spin relaxation of gaseous He^3, Phys. Rev. 179 (1969) 156–165.
[24] R.E. Jacob, B. Driehuys, B. Saam, Fundamental mechanisms of ^{3}He relaxation on glass, Chem. Phys. Lett. 370 (2003) 261–267.
[25] J. Schmiedeskamp, W. Heil, E.W. Otten, R.K. Kremer, A. Simon, J. Zimmer, Paramagnetic relaxation of spin polarized ^{3}He at bare glass surfaces, Eur. Phys. J. D 38 (2006) 427–438.
[26] B. Driehuys, G.D. Cates, W. Happer, Surface relaxation mechanisms of laser-polarized ^{129}Xe, Phys. Rev. Lett. 74 (1995) 4943–4946.
[27] D.M. Deaton, P.A. Cella, K.C. Hasson, D. Zollinger, B. Driehuys, Containers for hyperpolarized gases and associated methods, US Patent 6,128,918, 2000.
[28] W. Happer, E. Miron, S. Schaefer, D. Schreiber, W.A. van Wijngaarden, X. Zeng, Polarization of the nuclear spins of noble-gas atoms by spin exchange with optically pumped alkali-metal atoms, Phys. Rev. A 29 (1984) 3092–3110.
[29] B. Driehuys, G.D. Cates, E. Miron, K. Sauer, D.K. Walter, W. Happer, High-volume production of laser-polarized ^{129}Xe, Appl. Phys. Lett. 69 (1996) 1668–1670.
[30] S.T. Hwang, C.K. Choi, K. Kammermeyer, Gaseous transfer coefficients in membranes, Sep. Sci. 9 (1974) 461–478.
[31] H.E. Möller, X.J. Chen, M.S. Chawla, G.P. Cofer, B. Driehuys, L.W. Hedlund, S.A. Suddarth, G.A. Johnson, Sensitivity and resolution in 3D NMR microscopy of the lung with hyperpolarized noble gases, Magn. Reson. Med. 41 (1999) 800–808.
[32] H.E. Möller, Z.I. Cleveland, L.W. Hedlund, B. Fubara, G.P. Cofer, B. Driehuys, Direct gas infusion of hyperpolarized ^{129}Xe into blood—a new approach to imaging pulmonary perfusion and gas exchange, in: Proceedings of the 17th Annual Meeting of ISMRM, Honolulu, HI, USA, 2009, p. 2205.
[33] Z.I. Cleveland, H.E. Möller, L.W. Hedlund, J. Nouls, M. Freeman, Y. Qi, B. Driehuys, 3D imaging of pulmonary ventilation and perfusion in rats using hyperpolarized ^{129}Xe. in: Proceedings of the 19th Annual Meeting of ISMRM, Montréal, QC, Canada, 2011, p. 883.